

# Controlling the shape of small clusters with and without macroscopic fields

Francesco Boccardo\* and Olivier Pierre-Louis†

*Institut Lumière Matière, UMR5306 Université Lyon 1 - CNRS, 69622 Villeurbanne, France*

(Dated: May 19, 2022)

Despite major advances in the understanding of the formation and dynamics of nano-clusters in the past decades, theoretical bases for the control of their shape are still lacking. We investigate strategies for driving fluctuating few-particle clusters to an arbitrary target shape in minimum time with or without an external field. This question is recast into a first passage problem, solved numerically, and discussed within a high temperature expansion. Without field, large-enough low-energy target shapes exhibit an optimal temperature at which they are reached in minimum time. We then compute the optimal way to set an external field to minimize the time to reach the target, leading to a gain of time that grows when increasing cluster size or decreasing temperature. This gain can shift the optimal temperature or even create one. Our results could apply to clusters of atoms at equilibrium, and colloidal or nanoparticle clusters under thermo- or electrophoresis.

Less than a decade after its discovery [1], scanning tunneling microscope (STM) was used to position atoms on a surface with Ångstrom precision [2], reaching atomic-scale control on the organization of matter. Following this seminal work, many examples of organization of atoms [3, 4], molecules or nanoparticles [5–9] and colloids [10, 11] were obtained with tools like STM, atomic force microscope, or optical tweezers. However, important challenges are still open in the control of few-particle clusters.

The first one is to control matter at the nanoscale with an external macroscopic field that does not act on one single particle or atom at a time, but on the whole cluster. External fields such as light acting on metal nanoparticle clusters [12] or electromigration acting on atomic monolayer clusters [13–16] are known to lead to complex equilibrium or non-equilibrium cluster shapes. However, these shapes are only a very small fraction of all possible shapes, that are dictated by the physics of the interaction of the driving force with the system.

Another challenge lies in the ability to obtain refined control of nanostructure shapes in the presence of thermal fluctuations that activate the random diffusion of particles and atoms, leading to shape fluctuations [15, 17, 18]. Some progress in this direction has been achieved with the control of the formation and order of colloidal clusters [19–21] in finite-temperature experiments. However, the control of the cluster shape is still an open issue.

In order to address these challenges, we investigate strategies to reach arbitrary cluster shapes in minimum time in the presence of fluctuations. We focus on the control of few-particles two-dimensional clusters and find how a given target shape can be reached in minimum time with and without macroscopic external field. This problem which is formulated as the minimization of a first passage time on the graph of cluster configurations, is solved numerically and studied analytically with the help of a high temperature expansion.

In the absence of field, we find that large compact target shapes exhibit an optimal temperature at which they can be reached in minimum time. In the presence of

an external field we use dynamic programming [22, 23] to find the optimal way to set the external field as a function of the cluster shape to reach the target in minimum time. The gain in time due to the forces increases with decreasing temperature and with increasing clusters size. This gain can shift the optimal temperature, or create one when it does not exist in the absence of forces.

We focus on clusters with edge diffusion dynamics. Edge diffusion was observed in metal atomic monolayer islands [24, 25], and for colloids [26]. However, our strategy can readily be extended to any type of dynamics that preserve the number of particles such as surface-diffusion dynamics inside vacancy clusters [27–29], or dislocation-mediated cluster rearrangements in colloids [30] and metal nanoclusters [31, 32]. We discuss possible experiments with clusters of atoms or colloids.

**Model.** We consider a small cluster on a square lattice with lattice parameter  $a$  and nearest-neighbor bonds  $J$  under an external macroscopic force  $\mathbf{F}$ . We assume that the current configuration of the cluster, hereafter denoted as the state  $s$ , can be observed at all times. The force is chosen as a function of  $s$ . This choice is encoded in the policy  $\phi$ , so that  $\mathbf{F} = \phi(s)$ . The state  $s$  can change to another state  $s'$  via the motion of a single particle to one of its nearest or next-nearest neighbor sites along the cluster edge. Moves that break the cluster are forbidden. Following usual models for biased diffusion [15, 33, 34], the hopping rate is assumed to take an Arrhenius form

$$\gamma_{\phi}(s, s') = \nu \exp[-(n_{ss'}J - \phi(s) \cdot \mathbf{u}_{ss'})/k_B T], \quad (1)$$

where  $k_B T$  is the thermal energy and  $\nu$  is an attempt frequency,  $n_{ss'}$  is the number of in-plane nearest neighbors in state  $s$  before hopping. To gain computation time, we freeze atoms with  $n_{ss'} = 4$ . In addition, we assume that the displacement vector to the diffusion saddle point  $\mathbf{u}_{ss'}$  is half the displacement vector between the initial and final positions of the moving atom [15]. In the following, we choose units where  $k_B = 1$ ,  $J = 1$ ,  $\nu = 1$  and  $a = 1$ .

Our goal is to study the time to reach a target cluster configuration  $\bar{s}$  from an initial state  $s$ . This time can be

seen as a first passage time  $\tau_\phi(s, \bar{s})$  in a random walk on the graph of cluster configurations [35, 36], as represented in Fig. 1. Since the dynamics is Markovian,  $\tau_\phi(s, \bar{s})$  is equal to the expected residence time  $t_\phi(s)$  in state  $s$  plus the first passage time from the new state  $s'$  after the move [37]. Considering all possible moves, we obtain a recursion relation

$$\tau_\phi(s, \bar{s}) = t_\phi(s) + \sum_{s' \in \mathcal{B}_s} p_\phi(s, s') \tau_\phi(s', \bar{s}), \quad (2)$$

where  $p_\phi(s, s') = \gamma_\phi(s, s') t_\phi(s)$  is the transition probability from  $s$  to  $s'$ ,  $t_\phi(s) = 1 / \sum_{s' \in \mathcal{B}_s} \gamma_\phi(s, s')$ , and  $\mathcal{B}_s$  the set of states that can be reached from  $s$  via a single move. Relation Eq. (2) is supplemented with the boundary condition  $\tau_\phi(\bar{s}, \bar{s}) = 0$ .

We also define the expected return time to target, i.e. spent outside the target before returning to it when starting from the target itself [38]

$$\tau_\phi^r(\bar{s}) = \sum_{s \in \mathcal{B}_{\bar{s}}} p_\phi(\bar{s}, s) \tau_\phi(s, \bar{s}). \quad (3)$$

For the sake of concision, we mainly focus on the analysis of  $\tau_\phi^r(\bar{s})$  instead of  $\tau_\phi(s, \bar{s})$  which is different for each  $s$ .

**Zero force.** Let us first set the force to zero in all states,  $\phi(s) = \mathbf{0}$ . This leads to standard equilibrium fluctuation dynamics that have been investigated thoroughly in the case of edge diffusion [17, 18, 24]. Although some quantities related to first passage processes have been discussed within the frame of persistence of fluctuations [39, 40], there is to our knowledge no study of the

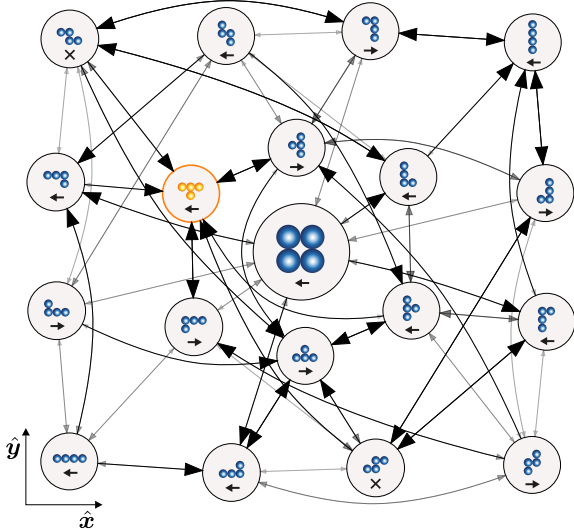


Figure 1. Graph of configurations for a tetramer cluster ( $N = 4$ ) at  $T = 0.24$ . The node size is proportional to the expected residence time  $t_\phi(s)$ . The thickness and shade of the edges are proportional to the transition probability  $p_\phi(s, s')$ . Arrows in the nodes represent an optimal policy  $\phi_*(s)$  to reach the orange target shape (crosses correspond to a zero force).

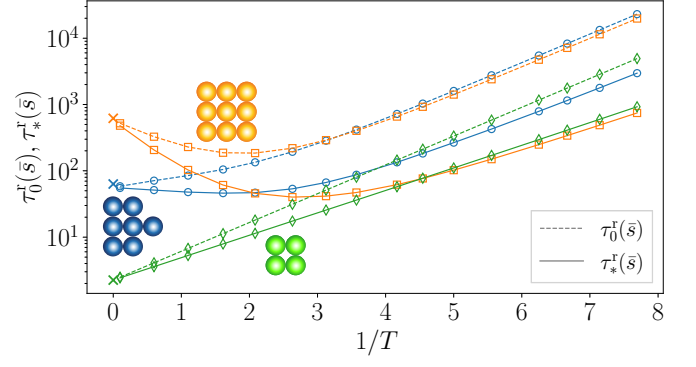


Figure 2. Expected return time to target as a function of  $1/T$ . Zero-force case  $\tau_0^r(\bar{s})$  and under the optimal policy  $\tau_*^r(\bar{s})$  with  $F_0 = 0.4$ . The  $\times$  correspond to  $\tau_\infty^r(\bar{s})$  for  $T \rightarrow \infty$ .

first passage times to cluster configurations. We have evaluated  $\tau_\phi(s, \bar{s})$  numerically using the method of iterative evaluation [22]: for a given  $\bar{s}$ , we iterate the evaluation of  $\tau_\phi(s, \bar{s})$  by substitution of its value in the right hand side of Eq. (2). Since it requires to list all states, such a method is suitable for small clusters, which corresponds to our focus in this Letter. Indeed, the total number  $S_N$  of configurations for a cluster with  $N$  particles, often called polyominoes or lattice animals [41], grows exponentially with  $N$ :  $S_N \sim c\lambda^N/N$ , with  $\lambda \approx 4.0626$  and  $c \approx 0.3169$  [42]. We have performed simulations with  $N \leq 12$ , with  $S_{12} \approx 5 \times 10^5$  states.

The resulting expected return time to target with zero force  $\tau_0^r(\bar{s})$  is shown in Fig. 2 as a function of  $1/T$ . For small clusters,  $\tau_0^r(\bar{s})$  increases monotonously as the temperature is decreased. This is expected because thermally activated hopping diffusion events become slower at low temperatures. However,  $\tau_0^r(\bar{s})$  exhibits a minimum as a function of temperature for clusters that are larger and more compact. As shown in [Supp. Mat.](#), a similar minimum is found in the time  $\tau_0(s, \bar{s})$  to reach the target starting from any state  $s$ . This striking result implies that some targets exhibit an optimal temperature at which the target can be reached in minimum time.

The presence of a minimum is associated to a change of slope of  $\tau_0^r(\bar{s})$  as a function of  $1/T$  at high temperatures. We therefore study the high temperature behavior in more details. In the limit  $T \rightarrow \infty$ , the rates (1) are independent of the initial and final state and of the force:  $\gamma_\phi(s, s') \rightarrow 1$ . As a consequence,  $\tau_\phi^r(\bar{s})$  is independent of the policy  $\phi$  at infinite temperature  $\tau_\phi^r(\bar{s}) \rightarrow \tau_\infty^r(\bar{s})$ . A simple result is known from the literature [43] (see also [Supp. Mat.](#)) when all rates are equal:  $\tau_\infty^r(\bar{s}) = (S_N - 1)/d_{\bar{s}}$ , where the degree  $d_{\bar{s}}$  of the target is the number of states that can be reached from the target  $\bar{s}$  in one move. This quantity is similar to the lower bound of the mean first passage time (averaged over all initial states  $s$ ), which is often used to characterize first passages in random graphs [44–47].

When the temperature is decreased, the moves become

sensitive to the energy. From detailed balance, a move that leads to a decrease of energy is faster than the reverse move. As a consequence, the cluster goes faster towards states with lower energy. Thus, the time to reach the target decreases if the target has a lower energy. However, this trend is only describing relative variations of the time to reach different targets. When decreasing the temperature, there is also a global slowing-down of the dynamics because of the Arrhenius dependence of the rates on temperature in Eq. (1). The decrease or increase of first passage times to the target—or equivalently of  $\tau_\phi^r(\bar{s})$ —depends on the competition between these two effects: relative energy effect vs global slowing down.

This competition can be analyzed from a high temperature expansion to first order in  $1/T$  (details are reported in **Supp. Mat.**), leading to

$$\tau_\phi^r(\bar{s}) = \left(1 + \frac{M_0(\bar{s})}{T}\right) \tau_\infty^r(\bar{s}), \quad (4)$$

$$M_0(\bar{s}) = \frac{1}{1 - S_N^{-1}} \left\langle \tilde{\delta}_{s\bar{s}} \langle n_{ss'} \rangle_{\bar{s}} - d_s g_n(s, \bar{s}) \right\rangle_{s \in \mathcal{S}}, \quad (5)$$

where  $\tilde{\delta}_{ss'} = 1 - \delta_{ss'}$  with  $\delta$  the Kronecker symbol,  $\langle \cdot \rangle_{s \in \mathcal{Z}}$  indicates the average over the states in the set of states  $\mathcal{Z}$ , and  $\mathcal{S}$  is the set of all states. We also use the notation  $\langle \cdot \rangle_{\bar{s}} = \langle \cdot \rangle_{s' \in \mathcal{B}_{\bar{s}}}$ . In addition, the local covariance of any quantity  $q_{ss'}$  with  $\tau_\infty(s, \bar{s})$  is defined as

$$g_q(s, \bar{s}) = \left\langle (q_{ss'} - \langle q_{ss'} \rangle_{\bar{s}})(\tau_\infty(s', \bar{s}) - \langle \tau_\infty(s', \bar{s}) \rangle_{\bar{s}}) \right\rangle_{\bar{s}},$$

where  $\langle \cdot \rangle_{\bar{s}} = \langle \cdot \rangle_{s' \in \mathcal{B}_{\bar{s}}}$ . In Fig. 3(a), we see that Eq. (5) is in good agreement with the value  $M_0^{\text{sim}}(\bar{s})$  obtained from a high temperature fit of the numerical solution from iterative evaluation (small deviations are caused by the freezing of 4-neighbors particles).

In Eq. (5), the first term proportional to  $\langle n_{ss'} \rangle_{\bar{s}}$  accounts for the global slowing down of the dynamics, while the second term proportional to  $d_s g_n(s, \bar{s})$  accounts for the relative energy effect. The global slowing down contribution can be approximated by  $\rho_0(N) = \langle \langle n_{ss'} \rangle_{\bar{s}} \rangle_{s \in \mathcal{S}}$ , which converges exponentially to  $\rho_0(\infty) \approx 1.64$  for large  $N$  (see **Supp. Mat.** for details). The relative energy effect is dominated by moves from  $\mathcal{B}_{\bar{s}}$  to the target  $\langle n_{s\bar{s}} - \langle n_{ss''} \rangle_{\bar{s}} \rangle_{\bar{s}}$ , where  $\langle \cdot \rangle_{\bar{s}} = \langle \cdot \rangle_{s \in \mathcal{B}_{\bar{s}}}$ . This relation is derived and checked in **Supp. Mat.** We therefore obtain

$$M_0^{\text{appr}}(\bar{s}) = \rho_0(N) + \rho_1 \langle n_{s\bar{s}} - \langle n_{ss''} \rangle_{\bar{s}} \rangle_{\bar{s}}, \quad (6)$$

where  $\rho_1 \approx 1.60$ . As shown in Fig. 3(a),  $M_0^{\text{appr}}(\bar{s})$  provides a fair approximation to  $M_0(\bar{s})$ . The dispersion originates from assumptions of uncorrelation of  $\tau_\infty$  with  $n_{ss'}$ , and of variations of  $\tau_\infty$  dominated by the difference between  $\tau_\infty(\bar{s}, \bar{s}) = 0$  on the target and  $\tau_\infty(s, \bar{s})$  in

its neighborhood  $\mathcal{B}_{\bar{s}}$ . The sign of  $M_0^{\text{appr}}(\bar{s})$  can serve as a simple guide to the presence of a minimum as a function of  $T$ , i.e. an optimal temperature, and also makes explicit the link between the minimum and the compactness of the target. For example, in a linear one-atom-thick target, only the two atoms at the tips can move, so that  $\langle n_{s\bar{s}} \rangle_{\bar{s}} = 1$  and an inspection of the possible moves shows that  $\langle \langle n_{ss''} \rangle_{\bar{s}} \rangle_{\bar{s}} = 4/3$ . This leads to  $M_0^{\text{appr}}(\bar{s}) = \rho_0(N) - \rho_1/3 \approx 0.9 > 0$  for  $N = 7$ , in agreement with  $M_0^{\text{sim}}(\bar{s}) \approx 1.04$  found by iterative evaluation. In contrast, in the limit of large compact (square, rectangular, etc) islands, for which  $\langle n_{s\bar{s}} \rangle_{\bar{s}} = 1$  and  $\langle \langle n_{ss''} \rangle_{\bar{s}} \rangle_{\bar{s}} \rightarrow 3$ , we obtain  $M_0^{\text{appr}}(\bar{s}) = -1.57 < 0$  leading to a minimum.

Note however that the convergence of value iteration is difficult not only for large clusters, but also for high-energy (i.e., non-compact) target shapes when the temperature is decreased. Indeed, disparate times-scales have to be resolved (fast relaxation towards low-energy shapes vs large time to reach high-energy shapes).

**Optimal policy in the presence of forces.** Our goal now is to determine the optimal policy  $\phi_*$  that minimizes  $\tau_\phi(s)$ , and the resulting optimal first passage time  $\tau_*(s, \bar{s}) = \min_\phi \tau_\phi(s, \bar{s})$  for non-zero forces. Such a problem, called a Markov decision process, can be solved using well-known dynamic programming methods [22, 23]. We substitute the optimal policy in Eq. (2) to obtain the so-called Bellmann optimality equation

$$\tau_*(s, \bar{s}) = \min_{\phi(s)} \left[ t_\phi(s) + \sum_{s' \in \mathcal{B}_s} p_\phi(s, s') \tau_*(s', \bar{s}) \right]. \quad (7)$$

As in the zero-force case, we iterate Eq.(7). However minimization over the force in  $s$  is taken at each iteration. This method, called value iteration, provides both  $\tau_*(s, \bar{s})$  and the optimal policy  $\phi_*$ . Due to the fast increase of

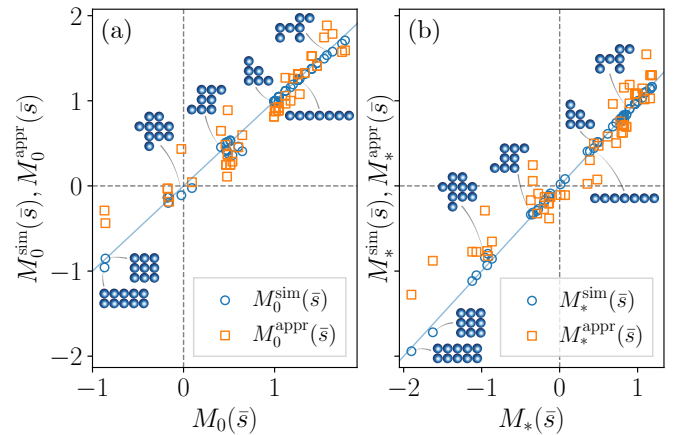


Figure 3. Estimates of the high temperature slope.  $M_0(\bar{s})$  and  $M_*(\bar{s})$  correspond to the analytical expressions of Eqs. (5,8).  $M_0^{\text{sim}}(\bar{s})$  and  $M_*^{\text{sim}}(\bar{s})$  are the slopes extracted from a high temperature fit using iterative numerical methods.  $M_0^{\text{appr}}(\bar{s})$  and  $M_*^{\text{appr}}(\bar{s})$  are approximate expressions from Eqs. (6,9).

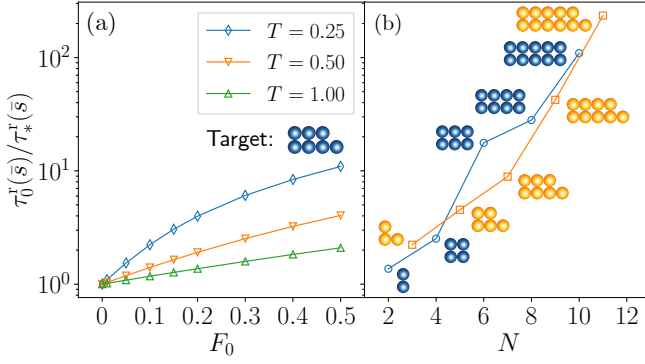


Figure 4. Gain  $\tau_0^r(\bar{s})/\tau_*^r(\bar{s})$  in the return time to target due to the optimization of the forces. (a) As a function of the force magnitude  $F_0$ , for a fixed target at different  $T$ . (b) For similar targets of increasing size, with  $T = 0.24$  and  $F_0 = 0.4$ .

$S_N$  with  $N$ , its computational cost grows exponentially with  $N$  (see [Supp. Mat.](#)).

We choose a force  $\mathbf{F}$  that is always oriented in  $\hat{\mathbf{x}}$  direction ((10) lattice direction), with 3 possible values:  $\{-F_0\hat{\mathbf{x}}, \mathbf{0}, F_0\hat{\mathbf{x}}\}$ , with  $F_0 > 0$ . An example of optimal policy is shown in Fig. 1. As an important remark, the force can drive the cluster towards any target shape even if the symmetries of the target are not compatible with those of the force because observation itself (i.e. the knowledge of  $s$ ) breaks the symmetry.

The gain due to the optimal policy is reported in Fig. 4, using the zero-force policy as a reference. In [Supp. Mat.](#), we show that using a random-force policy as a reference leads to similar results. As seen from Fig. 4(a), the gain increases not only when  $F_0$  is increased, but also when  $T$  is decreased. This is intuitively expected since the relative change between different rates due to a change of the force increases when  $F_0/T$  is increased. In addition, the gain increases when the size of the cluster increases, as shown in Fig. 4(b). A naive explanation for this trend is that an increase of  $N$  leads to an increase of the number of states  $S_N$ , and therefore to an increase of the number of ways to tune the policy  $\phi$  in order to minimize  $\tau_\phi(s, \bar{s})$ .

Again, a high temperature expansion leads to (derivation reported in [Supp. Mat.](#))

$$\tau_*^r(\bar{s}) = \left(1 + \frac{M_*(\bar{s})}{T}\right) \tau_\infty^r(\bar{s}), \quad (8)$$

$$M_*(\bar{s}) = M_0(\bar{s}) - \frac{F_0}{1 - S_N^{-1}} \left\langle \left| \tilde{\delta}_{s\bar{s}} \langle u_{ss'} \rangle_I - d_s g_u(s, \bar{s}) \right| \right\rangle_{s \in \mathcal{S}},$$

where  $u_{ss'} = \mathbf{u}_{ss'} \cdot \hat{\mathbf{x}}$ . The numerical solution of Eq. (7) is in agreement with Eq. (8) (up to small deviations due to 4-neighbors particle freezing, see [Supp. Mat.](#)).

Two remarks are in order. First,  $\langle u_{ss'} \rangle_I$  is small and its contribution to the term proportional to  $F_0$  in Eq. (8) is negligible. Second, the absolute value forbids the cancellation of contributions with randomly different signs, leading to a behavior which is qualitatively different from

that of  $M_0(\bar{s})$ . Indeed, the average is not dominated by the largest terms coming from the strong change of  $\tau_\infty(s, \bar{s})$  between the target and its first neighbors, but by the typical values of  $|d_s g_u(s, \bar{s})|$  in all states. Based on this observation, a detailed analysis reported in [Supp. Mat.](#) leads to the approximation

$$M_*^{\text{appr}}(\bar{s}) = M_0(\bar{s}) - \frac{2^{1/2}}{\pi^{1/2}} F_0 \sigma_u \sigma_{\tau_\infty}(\bar{s}) \langle d_s^{1/2} \rangle_{s \in \mathcal{S}}, \quad (9)$$

where we have defined the standard deviations

$$\sigma_u = \left\langle \left( (u_{ss'} - \langle u_{ss'} \rangle_I)^2 \right)^{1/2} \right\rangle_{s \in \mathcal{S}}, \quad (10)$$

$$\sigma_{\tau_\infty}(\bar{s}) = \left\langle \left( (\tau_\infty(s', \bar{s}) - \langle \tau_\infty(s'', \bar{s}) \rangle_I)^2 \right)^{1/2} \right\rangle_{s \in \mathcal{S}}. \quad (11)$$

In Fig. 3, the approximation Eq.(9) is seen to be valid up to some dispersion originating mainly in the assumption of uncorrelation between  $u_{ss'}$  and  $\tau_\infty$ .

While  $\langle n_{s\bar{s}} - \langle n_{ss''} \rangle_I \rangle_-$  and  $\sigma_u$  are bounded because  $1 \leq n_{ss'} \leq 4$  and  $-1/2 \leq -u_{ss'} \leq 1/2$ , the quantities  $\sigma_{\tau_\infty}(\bar{s})$  and  $\langle d_s^{1/2} \rangle_{s \in \mathcal{S}}$  grow with  $N$  (see [Supp. Mat.](#)). Hence, from Eq. (6),  $M_0^{\text{appr}}(\bar{s})$  is bounded and the contribution proportional to  $F_0$  in Eq. (9) usually dominates over the term  $M_0(\bar{s})$  for large  $N$ . Thus, when  $N$  is large enough,  $M_*(\bar{s})$  should be negative and an optimal temperature should be generically present. This trend is confirmed by Fig. 3(b). Simulations with  $N = 12$  and  $F_0 = 0.4$  (reported in Fig. 10 of [Supp. Mat.](#)) also confirm the generic presence of a minimum for larger targets.

**Discussion.** For atomic metals clusters where edge diffusion is observed (Ag, Cu, etc.), estimates of the edge diffusion barrier  $\sim J$  or kink energies  $\sim J/2$  suggest that  $J \approx 0.2$  to  $0.3$  eV [24, 48–51]. For the square 9-atom target depicted in Fig.2 the optimal temperature corresponds to  $J/k_B T \approx 2$ . Choosing  $J = 0.2$  eV we obtain an optimal temperature  $\approx 10^3$  K which is too high to be observed in usual experiments. Thus,  $\tau_0(s, \bar{s})$  should decrease with temperature in usual experimental conditions. If needed, a quench can also be used to freeze the cluster once the target shape is reached. However, using electromigration as an external force leads to [25]  $F_0 a/J \approx 10^{-4}$ , which is too small to allow for the control of few-atoms clusters.

Edge diffusion can also be observed with colloids [26]. Using colloids with depletants,  $J \sim \text{few } k_B T$  [52]. The optimal temperature should then be observable in the absence of force. Thermophoretic forces [53–55] for polystyrene beads of radius  $2.5 \mu\text{m}$  are  $\sim 10 k_B T/\mu\text{m}$  [53]. Hence, micron-size colloids can lead to  $F_0 a/J \sim 1$ , which allows for shape control by a macroscopic force.

However, most experiments on colloid clusters report mass transport dominated by attachment-detachment at the edges [56]. Our analysis can be adapted to vacancy clusters [5, 57, 58] with volume-preserving detachment-diffusion-reattachment events. Moreover, other two or three-dimensional lattices also could be analyzed. Furthermore, multi-particle and off-lattice processes (such as

those involved in dislocation-mediated dynamics) can be included as long as they are pre-determined (using e.g. energy-exploration methods) and their number is finite, to allow for the numerical solution of Eqs. (2) and (7). Since the presence of the minimum depends only on the generic competition between the relative energy effect and global slowing down, we speculate that it should not depend on the details of mass transport kinetics.

In conclusion, thermal fluctuations can be used to reach desired nano-cluster shapes. There is a temperature that minimizes the time to reach large-enough and compact shapes. Furthermore, macroscopic fields can help gaining orders of magnitude in the time to reach arbitrary shapes. We hope that our work will motivate experimental investigations for the control of atomic and colloidal clusters, and will open theoretical directions for the optimization of first passage times on graphs.

---

\* francesco.boccardo@univ-lyon1.fr

† olivier.pierre-louis@univ-lyon1.fr

- [1] G. Binnig and H. Rohrer, *Surf. Sci.* **126**, 236 (1983).
- [2] D. M. Eigler and E. K. Schweizer, *Nature* **344**, 524 (1990).
- [3] A. Cooper, J. P. Covey, I. S. Madjarov, S. G. Porsev, M. S. Safronova, and M. Endres, *Phys. Rev. X* **8**, 041055 (2018).
- [4] D. Barredo, S. de Léséleuc, V. Lienhard, T. Lahaye, and A. Browaeys, *Science* **354**, 1021 (2016).
- [5] A. Martínez-Galera, I. Brihuega, A. Gutiérrez-Rubio, T. Stauber, and J. Gómez-Rodríguez, *Sci. Rep.* **4**, 1 (2014).
- [6] D. Erickson, X. Serey, Y.-F. Chen, and S. Mandal, *Lab Chip* **11**, 995 (2011).
- [7] T. Junno, K. Deppert, L. Montelius, and L. Samuelson, *Appl. Phys. Lett.* **66**, 3627 (1995).
- [8] C. Baur, A. Bugacov, B. E. Koel, A. Madhukar, N. Montoya, T. R. Ramachandran, A. A. G. Requicha, R. Resch, and P. Will, *Nanotechnology* **9**, 360 (1998).
- [9] F. J. Rubio-Sierra, W. M. Heckl, and R. W. Stark, *Adv. Eng. Mater.* **7**, 193 (2005).
- [10] P. T. Korda, M. B. Taylor, and D. G. Grier, *Phys. Rev. Lett.* **89**, 128301 (2002).
- [11] D. G. Grier, *Nature* **424**, 810 (2003).
- [12] P. McCormack, F. Han, and Z. Yan, *J. Phys. Chem. Lett.* **9**, 545 (2018).
- [13] P. Kuhn, J. Krug, F. Hausser, and A. Voigt, *Phys. Rev. Lett.* **94**, 166105 (2005).
- [14] M. Mahadevan and R. M. Bradley, *Phys. Rev. B* **59**, 11037 (1999).
- [15] O. Pierre-Louis and T. L. Einstein, *Phys. Rev. B* **62**, 13697 (2000).
- [16] S. Curiotto, F. Leroy, P. Müller, F. Cheynis, M. Michailov, A. El-Barraj, and B. Ranguelov, *J. Cryst. Growth* **520**, 42 (2019).
- [17] S. V. Khare, N. C. Bartelt, and T. L. Einstein, *Phys. Rev. Lett.* **75**, 2148 (1995).
- [18] K. C. Lai, D.-J. Liu, and J. W. Evans, *Phys. Rev. B* **96**, 235406 (2017).
- [19] J. J. Juárez and M. A. Bevan, *Adv. Funct. Mater.* **22**, 3833 (2012).
- [20] J. J. Juárez, P. P. Mathai, J. A. Liddle, and M. A. Bevan, *Lab Chip* **12**, 4063 (2012).
- [21] Y. Xue, D. J. Beltran-Villegas, X. Tang, M. A. Bevan, and M. A. Grover, *IEEE Trans. Control Syst. Technol.* **22**, 1956 (2014).
- [22] R. S. Sutton and A. G. Barto, *Reinforcement Learning: An Introduction*, 2nd ed. (The MIT Press, 2018).
- [23] R. E. Bellman, *Dynamic Programming* (Dover Publications, Inc., USA, 2003).
- [24] M. Giesen, *Prog. Surf. Sci.* **68**, 1 (2001).
- [25] C. Tao, W. G. Cullen, and E. D. Williams, *Science* **328**, 736 (2010).
- [26] B. C. Hubartt and J. G. Amar, *J. Chem. Phys.* **142**, 024709 (2015).
- [27] R. Plass, J. A. Last, N. Bartelt, and G. Kellogg, *Nature* **412**, 875 (2001).
- [28] J. Heinonen, I. Koponen, J. Merikoski, and T. Ala-Nissila, *Phys. Rev. Lett.* **82**, 2733 (1999).
- [29] F. Leroy, A. El Barraj, F. Cheynis, P. Müller, and S. Curiotto, *Phys. Rev. B* **102**, 235412 (2020).
- [30] B. VanSaders and S. C. Glotzer, *Proc. Natl. Acad. Sci. U.S.A* **118**, e2017377118 (2021).
- [31] R. Huang, Y. Wen, A. F. Voter, and D. Perez, *Phys. Rev. Materials* **2**, 126002 (2018).
- [32] O. Trushin, P. Salo, M. Alatalo, and T. Ala-Nissila, *Surf. Sci.* **482-485**, 365 (2001).
- [33] S. Glasstone, K. J. Laidler, and H. Eyring, *The Theory of Rate Processes: The Kinetics of Chemical Reactions, Viscosity, Diffusion and Electrochemical Phenomena*, International chemical series (McGraw-Hill Book Company, Inc., 1941).
- [34] D.-J. Liu and J. D. Weeks, *Phys. Rev. B* **57**, 14891 (1998).
- [35] J. R. Sanchez and J. W. Evans, *Phys. Rev. B* **59**, 3224 (1999).
- [36] N. Combe and H. Larralde, *Phys. Rev. B* **62**, 16074 (2000).
- [37] N. G. Van Kampen, *Stochastic processes in physics and chemistry* (Elsevier, 1992).
- [38] As a technical remark, this definition requires to extend the policy and define a force on the target state itself. However, due to the Markovian character of the dynamics, this does not affect the mean first passage time to target and the optimal policy in the other states outside the target.
- [39] D. B. Dougherty, I. Lyubnitsky, E. D. Williams, M. Constantin, C. Dasgupta, and S. D. Sarma, *Phys. Rev. Lett.* **89**, 136102 (2002).
- [40] M. Constantin, S. Das Sarma, C. Dasgupta, O. Bondarchuk, D. B. Dougherty, and E. D. Williams, *Phys. Rev. Lett.* **91**, 086103 (2003).
- [41] A. J. Guttmann, *Polygons, Polyominoes and Polycubes*, Lecture Notes in Physics 775 (Springer, 2009).
- [42] I. Jensen and A. J. Guttmann, *J. Phys. A Math. Theor.* **33**, L257 (2000).
- [43] L. Lovász, *Combinatorics, Paul Erdős is eighty* **2**, 1 (1993).
- [44] Y. Lin, A. Julaiti, and Z. Zhang, *J. Chem. Phys.* **137**, 124104 (2012).
- [45] V. Tejedor, O. Bénichou, and R. Voituriez, *Phys. Rev. E* **80**, 065104 (2009).
- [46] A. Baronchelli and V. Loreto, *Phys. Rev. E* **73**, 026103 (2006).
- [47] J. D. Noh and H. Rieger, *Phys. Rev. Lett.* **92**, 118701 (2004).
- [48] R. Ferrando and G. Tréglia, *Phys. Rev. B* **50**, 12104

- (1994).
- [49] B. D. Yu and M. Scheffler, Phys. Rev. B **55**, 13916 (1997).
  - [50] H. Mehl, O. Biham, I. Furman, and M. Karimi, Phys. Rev. B **60**, 2106 (1999).
  - [51] R. Nelson, T. Einstein, S. Khare, and P. Rous, Surf. Sci. **295**, 462 (1993).
  - [52] J. Nozawa, S. Uda, S. Guo, A. Toyotama, J. Yamanaka, N. Ihara, and J. Okada, Cryst. Growth Des. **18**, 6078 (2018).
  - [53] L. Helden, R. Eichhorn, and C. Bechinger, Soft Matter **11**, 2379 (2015).
  - [54] M. Braibanti, D. Vigolo, and R. Piazza, Phys. Rev. Lett. **100** (2008).
  - [55] A. Würger, Rep. Prog. Phys. **73**, 126601 (2010).
  - [56] R. Ganapathy, M. R. Buckley, S. J. Gerbode, and I. Cohen, Science **327**, 445 (2010).
  - [57] P. García, R. Sapienza, A. Blanco, and C. López, Adv. Mater. **19**, 2597 (2007).
  - [58] J. A. Pariente, N. Caselli, C. Pecharromán, A. Blanco, and C. López, Small **16**, 2002735 (2020).



# Controlling the shape of small clusters with and without macroscopic fields: Supplemental Material

Francesco Boccardo\* and Olivier Pierre-Louis†

*Institut Lumière Matière, UMR5306 Université Lyon 1 - CNRS, 69622 Villeurbanne, France*

(Dated: May 19, 2022)

## I. EXPECTED RETURN TIME TO TARGET VS TIME TO TARGET FROM OTHER STATES

In the main text, we state that when the expected return time to target  $\tau_\phi^r(\bar{s})$  exhibits a minimum, the expected times to reach the target  $\tau_\phi(s, \bar{s})$  starting from any state  $s$  usually also exhibit a minimum. This is shown in Fig. 1 for two 9-atom targets, for the zero-force and under an optimal policy  $\phi_*$  with  $F_0 = 0.4$ . In both cases, the presence of a minimum both in  $\tau_\phi^r(\bar{s})$  and  $\tau_\phi(s, \bar{s})$  is clearly visible.

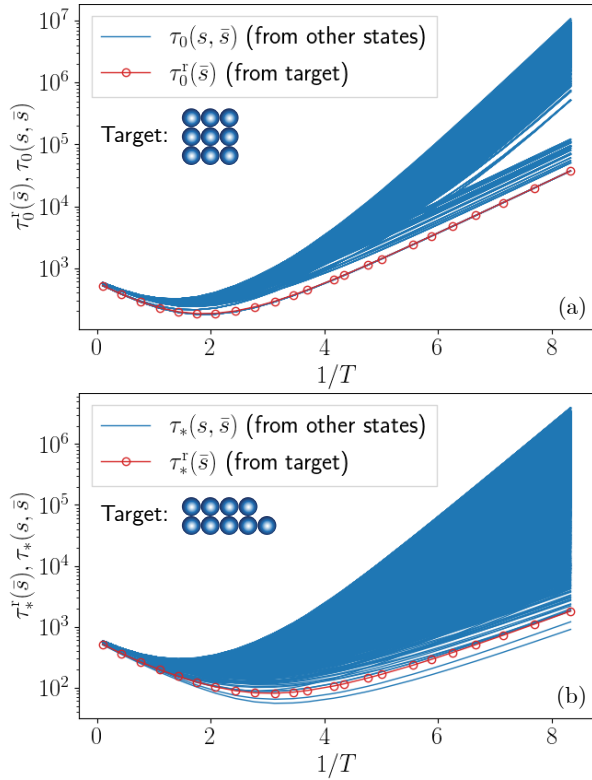


Figure 1. Expected time to reach the target as a function of  $1/T$ , starting from the target state itself (return time), and from all the other states in the system. (a) Zero-force case and (b) under an optimal policy  $\phi_*$ . The number of blue curves in these graphs is therefore equal to the number of states minus one (the target), i.e.  $S_9 - 1 = 9909$ .

## II. HIGH TEMPERATURE EXPANSION OF THE EXPECTED RETURN TIME TO TARGET

### A. Expression of the expected return time

Dividing the recursion relation Eq. (??) of the main text by  $t_\phi(s)$  and summing over all states but the target state, we obtain

$$\sum_s \frac{\tau_\phi(s, \bar{s})}{t_\phi(s)} = S_N - 1 + \sum_s \sum_{s' \in \mathcal{B}_s} \frac{p_\phi(s, s')}{t_\phi(s)} \tau_\phi(s', \bar{s}), \quad (1)$$

where  $\sum_s$  indicates the sum over all states in the system except for the target state  $\bar{s}$ , and  $\mathcal{B}_s$  is the set of bordering states of  $s$ , i.e. the states that can be reached from  $s$  in one physical move.

All physical moves except for those coming from the target are summed over in the last term of the right hand side of Eq. (1). Hence, we can invert the indices  $s$  and  $s'$  in the sum if we subtract the contribution of the moves starting from the target, leading to

$$\begin{aligned} \sum_s \frac{\tau_\phi(s, \bar{s})}{t_\phi(s)} &= S_N - 1 + \sum_s \sum_{s' \in \mathcal{B}_s} \frac{p_\phi(s', s)}{t_\phi(s')} \tau_\phi(s, \bar{s}) \\ &\quad - \sum_{s \in \mathcal{B}_{\bar{s}}} \frac{p_\phi(\bar{s}, s)}{t_\phi(\bar{s})} \tau_\phi(s, \bar{s}). \end{aligned} \quad (2)$$

The last term is proportional to the expected return time to target (Eq. (??) of the main text)

$$\tau_\phi^r(\bar{s}) = \sum_{s \in \mathcal{B}_{\bar{s}}} p_\phi(\bar{s}, s) \tau_\phi(s, \bar{s}). \quad (3)$$

We can therefore re-write Eq. (2) as

$$\begin{aligned} \tau_\phi^r(\bar{s}) &= t_\phi(\bar{s})(S_N - 1) \\ &\quad + t_\phi(\bar{s}) \sum_s \tau_\phi(s, \bar{s}) \left\{ \left( \sum_{s' \in \mathcal{B}_s} \frac{p_\phi(s', s)}{t_\phi(s')} \right) - \frac{1}{t_\phi(s)} \right\}. \end{aligned} \quad (4)$$

Then, writing  $t_\phi$  and  $p_\phi$  as a function of  $\gamma_\phi$ , we obtain an expression that is convenient for the study of the high temperature regime

$$\begin{aligned} \tau_\phi^r(\bar{s}) &= t_\phi(\bar{s})(S_N - 1) \\ &\quad + t_\phi(\bar{s}) \sum_s \tau_\phi(s, \bar{s}) \sum_{s' \in \mathcal{B}_s} (\gamma_\phi(s', s) - \gamma_\phi(s, s')), \end{aligned} \quad (5)$$

where we have dropped the exclusion of the target state (indicated by the bar) in the sum since  $\tau_\phi(\bar{s}, \bar{s}) = 0$ .

\* francesco.boccardo@univ-lyon1.fr

† olivier.pierre-louis@univ-lyon1.fr

### B. Infinite temperature limit

In the high temperature limit  $k_B T \rightarrow +\infty$ , the rates given by Eq. (??) of the main text all converge to the same value  $\gamma_\phi(s, s') \rightarrow 1$ , and therefore the residence time  $t_\phi(s) = 1/\sum_{s' \in \mathcal{B}_s} \gamma_\phi(s, s')$  reads

$$t_\phi(s) \rightarrow \frac{1}{d_s}, \quad (6)$$

where  $d_s$ , called the degree of state  $s$ , is the number of possible moves from  $s$ . Note that  $d_s$  is the cardinal of  $\mathcal{B}_s$ . As a consequence, Eq. (5) implies

$$\tau_\phi^r(\bar{s}) \rightarrow \tau_\infty^r(\bar{s}) = \frac{S_N - 1}{d_{\bar{s}}} \quad (7)$$

in the high temperature limit.

In addition, the general recursion relation Eq. (??) of the main text can be re-written as

$$1 = \sum_{s' \in \mathcal{B}_s} \gamma_\phi(s, s') (\tau_\phi(s, \bar{s}) - \tau_\phi(s', \bar{s})). \quad (8)$$

In the limit of infinite temperatures, this expression takes the form of the usual discretized Laplacian for the expected first passage times to the target  $\tau_\infty(s, \bar{s})$

$$1 = \sum_{s' \in \mathcal{B}_s} (\tau_\infty(s, \bar{s}) - \tau_\infty(s', \bar{s})). \quad (9)$$

This relation is valid everywhere but at the target state, where  $\tau_\infty(\bar{s}) = 0$ . The value of  $\tau_\infty(s, \bar{s})$  depends in general on the precise structure of the graph.

A vast literature is dedicated to the study of the first passage times on random graphs [1, 2]. However, most studies are devoted to the case where  $t_\phi(s) = 1$ , which is different from our infinite temperature limit. The difference lies only in the factor  $1/d_s$  in  $t_\phi(s)$ . A trace of this simple difference is that the mean first passage time (MFPT), which is the average of the first passage time over all initial states for a fixed target state, discussed in the literature with  $t_\phi(s) = 1$ , exhibits a lower bound [3, 4]  $\text{MFPT} \geq S_N \langle d_s \rangle / d_s$ , where  $\langle d_s \rangle$  is the average of  $d_s$  over all states. Up to the factor  $1/\langle d_s \rangle$ , this is identical to the expression of the expected return time to the target  $\tau_\phi^r(\bar{s})$  in Eq. (7).

### C. High temperature expansion

We perform an expansion to linear order in  $1/T$  to obtain the first correction to Eq. (7). We start with the expansion of the rates, defined in Eqs. (1,2) of the main text

$$\gamma_\phi(s, s') = 1 + \frac{1}{T} (-n_{ss'} + \varphi(s) u_{ss'}), \quad (10)$$

where we recall that  $n_{ss'}$  is the initial number of bonds of the atom which moves in the transition from state  $s$

to state  $s'$ . In addition, we have  $u_{ss'} = 1/2, 0, 0$  or  $-1/2$  when the move is in the direction  $+\hat{x}, -\hat{y}, +\hat{y}$  or  $-\hat{x}$  respectively. The  $+\hat{x}$  and  $+\hat{y}$  axes correspond to the (10) and (01) lattice directions respectively. Remark the symmetry relation  $u_{ss'} = -u_{s's}$ . Moreover,  $\varphi(s) = -F_0, 0$ , or  $F_0$  is the scalar force in state  $s$  given by the policy  $\phi$ , so that  $\phi(s) = \varphi(s) \hat{x}$ .

Inserting this expression in the expected return time Eq. (5), we obtain to linear order in  $1/T$

$$\begin{aligned} \tau_\phi^r(\bar{s}) &= \tau_\infty^r(\bar{s}) \left( 1 + \frac{M_\phi}{T} \right) \\ M_\phi &= \frac{1}{d_{\bar{s}}} \sum_{s \in \mathcal{B}_{\bar{s}}} (n_{\bar{s}s} - \varphi(\bar{s}) u_{\bar{s}s}) \\ &\quad + \frac{1}{S_N - 1} \sum_s \tau_\infty(s, \bar{s}) \sum_{s' \in \mathcal{B}_s} (n_{ss'} - n_{s's}) \\ &\quad + \frac{1}{S_N - 1} \sum_s \tau_\infty(s, \bar{s}) \sum_{s' \in \mathcal{B}_s} (\varphi(s') u_{s's} - \varphi(s) u_{ss'}), \end{aligned} \quad (11)$$

where the first passage time to target at infinite temperature  $\tau_\infty(s, \bar{s})$  is independent on the policy  $\phi$ . The normalized slope  $M_\phi$  obeys

$$\begin{aligned} (1 - \frac{1}{S_N}) M_\phi &= \left\langle (1 - \delta_{\bar{s}\bar{s}}) \langle n_{ss'} \rangle_{s' \in \mathcal{B}_s} - d_s g_n(s, \bar{s}) \right\rangle_{s \in \mathcal{S}} \\ &\quad - \left\langle \varphi(s) \left( (1 - \delta_{\bar{s}\bar{s}}) \langle u_{ss'} \rangle_{s' \in \mathcal{B}_s} - d_s g_u(s, \bar{s}) \right) \right\rangle_{s \in \mathcal{S}}, \end{aligned} \quad (12)$$

where  $\delta_{ss'}$  is the Kronecker symbol and the notation

$$\langle q_s \rangle_{s \in \mathcal{Z}} = \frac{1}{|\mathcal{Z}|} \sum_{s \in \mathcal{Z}} q_s \quad (13)$$

indicates the average of  $q_s$  taken over the states  $s$  belonging to the set of states  $\mathcal{Z}$  with cardinal  $|\mathcal{Z}|$ . In addition, we have defined the local covariances

$$\begin{aligned} g_n(s, \bar{s}) &= \left\langle \left( n_{ss'} - \langle n_{ss'} \rangle_{s'' \in \mathcal{B}_s} \right) \left( \tau_\infty(s', \bar{s}) - \langle \tau_\infty(s'', \bar{s}) \rangle_{s'' \in \mathcal{B}_s} \right) \right\rangle_{s' \in \mathcal{B}_s} \\ &\quad (14) \end{aligned}$$

$$\begin{aligned} g_u(s, \bar{s}) &= \left\langle \left( u_{ss'} - \langle u_{ss'} \rangle_{s'' \in \mathcal{B}_s} \right) \left( \tau_\infty(s', \bar{s}) - \langle \tau_\infty(s'', \bar{s}) \rangle_{s'' \in \mathcal{B}_s} \right) \right\rangle_{s' \in \mathcal{B}_s} \\ &\quad (15) \end{aligned}$$

that are averaged over the bordering states of  $s$ .

In the case of zero force, we set  $\varphi(s) = 0$  in Eq. (12) and readily obtain Eq. (7) of the main text.

We now consider the case of non-zero forces. Since  $\tau_\phi^r(\bar{s})$  is linear in the forces  $\varphi(s)$  from Eq. (12), we obtain the optimal policy  $\phi_*(s) = \varphi_*(s) \hat{x}$  from the sign of the prefactor of  $\varphi(s)$  in Eq. (12):

$$\varphi_*(s) = -F_0 \text{sign} [d_s g_u(s, \bar{s}) - \langle u_{ss'} \rangle_{s' \in \mathcal{B}_s}],$$

$$\varphi_*(\bar{s}) = -F_0 \text{sign} [g_u(\bar{s})]. \quad (16)$$



If the terms in the squared brackets vanish, then the contribution of the force term to  $\tau_\phi^r(\bar{s})$  is at least second order in  $1/T$ , and should therefore be negligible for high enough temperatures.

Using Eq. (16) in Eq. (12), we obtain the high temperature correction to the optimal expected return time to target

$$\left(1 - \frac{1}{S_N}\right)M_* = \left\langle (1 - \delta_{s\bar{s}}) \langle n_{ss'} \rangle_{s' \in \mathcal{B}_s} - d_s g_n(s, \bar{s}) \right\rangle_{s \in \mathcal{S}} - F_0 \left\langle \left| (1 - \delta_{s\bar{s}}) \langle u_{ss'} \rangle_{s' \in \mathcal{B}_s} - d_s g_u(s, \bar{s}) \right| \right\rangle_{s \in \mathcal{S}}, \quad (17)$$

which is identical to Eq. (??) of the main text.

#### D. Approximate expression of $M_0$

In Eq. (??) of the main text, the first term  $\langle (1 - \delta_{s\bar{s}}) \langle n_{ss'} \rangle_{s' \in \mathcal{B}_s} \rangle_{s \in \mathcal{S}}$  is the average over all possible states  $s$  except the target  $\bar{s}$  of the average number of bonds  $n_{ss'}$  that is broken to perform a move from  $s$ . This term essentially accounts for the global slowing down of the dynamics when the temperature is decreased. The number  $d_s$  of possible moves from a given state  $s$  grows moderately (like a power law) with  $N$ , as shown in Fig. 2, while the total number of states  $S_N$  grows exponentially with  $N$  as discussed in the main text. As a consequence, the contribution of the moves that start from the target is negligible when  $N$  is large enough. Hence, the first term in Eq. (??) of the main text can be approximated with the average  $\langle \langle n_{ss'} \rangle_{s' \in \mathcal{B}_s} \rangle_{s \in \mathcal{S}}$  of  $n_{ss'}$  over all states. Note that  $n_{ss'}$  is bounded ( $1 \leq n_{ss'} \leq 4$ ), and this average converges quickly to a value  $\rho_0$  around 1.64. A fit of  $\rho_0(N) = \langle \langle n_{ss'} \rangle_{s' \in \mathcal{B}_s} \rangle_{s \in \mathcal{S}}$  as for  $N > 2$ , provided in Fig. 3, shows that this convergence is exponential  $\rho_0(N) = \rho_0(\infty) - \tilde{\rho}_0 \exp(-N/N_0)$  with  $\tilde{\rho}_0 \approx 0.89$  and  $N_0 \approx 5.4$ .

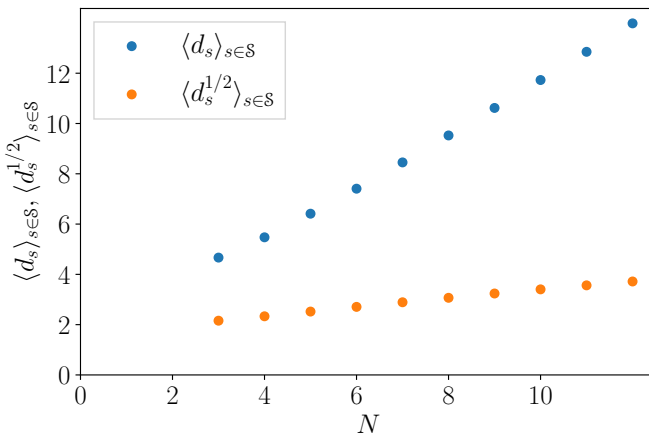


Figure 2. Mean of the degrees of the states  $d_s$  and their square roots over all states, for clusters of increasing size.

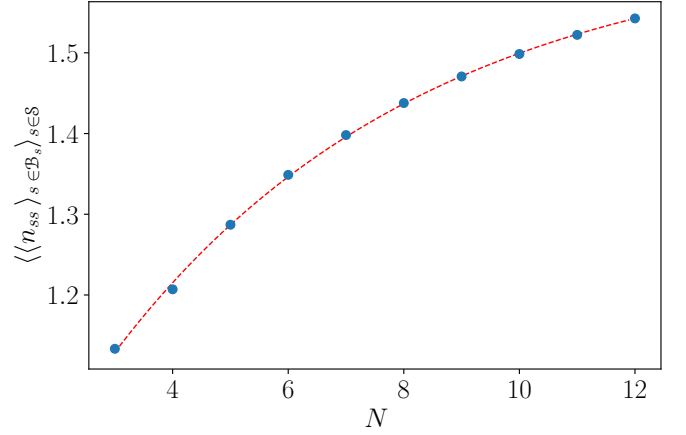


Figure 3. Mean of  $\langle n_{ss'} \rangle_{s' \in \mathcal{B}_s}$  over all states, for clusters of increasing size. The points are fitted with a decaying exponential, which gives an asymptotic value  $\rho_0(\infty) \approx 1.64$ .

The second term  $\langle d_s g_n(s, \bar{s}) \rangle_{s \in \mathcal{S}}$  in Eq. (??) of the main text accounts for the correlations between the number of bonds that are broken and the first passage time to target at infinite temperature when starting from a given state  $s$ . This second term accounts for the relative trend for the system to go faster towards low energy states. In order to analyze this expression, we introduce the concept of rings following Ref. [2]. The index of the rings  $m$  is defined as the minimum number of moves to reach the target. A ring  $\mathcal{R}_m$  is the ensemble of states with the same ring index  $m$ . Note that our definitions are such that  $\mathcal{R}_1 = \mathcal{B}_{\bar{s}}$ . The first passage time to target at infinite temperature  $\tau_\infty(s, \bar{s})$  is known to increase quickly up to an asymptotic value as  $m$  increases [2]. The asymptotic value is reached after a few rings. A plot of the mean first passage time to target as a function of the ring index is reported in Fig. 4. We therefore simply assume that the second term is dominated by the contributions related to the large variation of  $\tau_\infty(s, \bar{s})$  between the target state where  $\tau_\infty(\bar{s}, \bar{s}) = 0$  and the first ring.

When evaluating the term  $\langle d_s g_n(s, \bar{s}) \rangle_{s \in \mathcal{S}}$  in Eq. (17) we therefore need to sum only over the moves from states in  $\mathcal{B}_{\bar{s}}$ , which leads to

$$\langle d_s g_n(s, \bar{s}) \rangle_{s \in \mathcal{S}} \approx - \frac{d_{\bar{s}}}{S_N} \langle (n_{s\bar{s}} - \langle n_{ss''} \rangle_{s'' \in \mathcal{B}_s}) \tau_\infty(s, \bar{s}) \rangle_{s \in \mathcal{B}_{\bar{s}}}. \quad (18)$$

To obtain this relation, we have used the recursion relation Eq. (9), so that for the term with  $s' = \bar{s}$  and  $s \in \mathcal{B}_{\bar{s}}$  in Eq. (14), we have

$$\begin{aligned} \tau_\infty(s', \bar{s}) - \langle \tau_\infty(s'') \rangle_{s'' \in \mathcal{B}_s} &= \\ \tau_\infty(\bar{s}, \bar{s}) - \left( \tau_\infty(s, \bar{s}) - \frac{1}{d_s} \right) &= \\ - \left( \tau_\infty(s, \bar{s}) - \frac{1}{d_s} \right) &\approx -\tau_\infty(s, \bar{s}), \end{aligned}$$

where in the last line, we use  $1/d_s \ll \tau_\infty(s, \bar{s})$ , which is

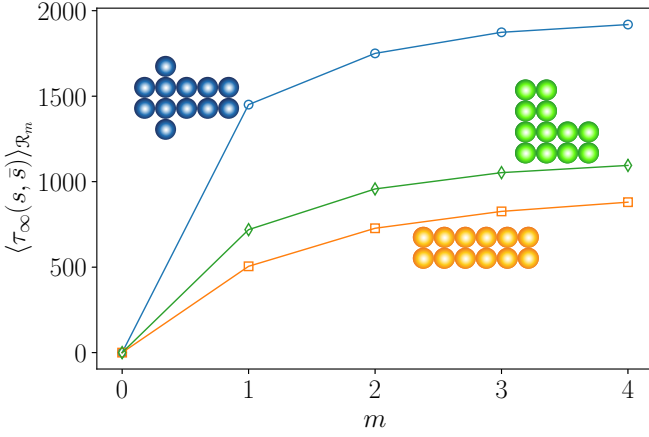


Figure 4. Mean on rings of the first passage time to target at infinite temperature as a function of the ring index  $m$  for three different targets with  $N = 12$ .

valid for  $N$  large enough. Finally, we simply assume the statistical independence of the two terms in the product in the brackets of Eq.(18), leading to

$$\langle d_s g_n(s, \bar{s}) \rangle_{s \in \mathcal{S}} \approx -\frac{d_{\bar{s}}}{S_N} \langle n_{s\bar{s}} - \langle n_{ss''} \rangle_{s'' \in \mathcal{B}_s} \rangle_{s \in \mathcal{B}_{\bar{s}}} \langle \tau_\infty(s, \bar{s}) \rangle_{s \in \mathcal{B}_{\bar{s}}}. \quad (19)$$

Since  $\langle \tau_\infty(s, \bar{s}) \rangle_{s \in \mathcal{B}_{\bar{s}}} = \tau_\infty^r(\bar{s}) = (S_N - 1)/d_{\bar{s}}$  and  $S_N \gg 1$ , we finally obtain

$$\langle d_s g_n(s, \bar{s}) \rangle_{s \in \mathcal{S}} \approx -\langle n_{s\bar{s}} - \langle n_{ss''} \rangle_{s'' \in \mathcal{B}_s} \rangle_{s \in \mathcal{B}_{\bar{s}}}. \quad (20)$$

This approximate relation is shown to be accurate in Fig. 5 up to a multiplicative factor  $\rho_1 \approx 1.60$  in the range of cluster sizes  $N = 2$  to 12 that we have explored. When the target shape is compact, then  $n_{s\bar{s}}$  is smaller than the average of  $n_{ss'}$  over the bordering states  $s'$  of the states  $s$  of the first ring. Hence, compact shapes lead to a positive contribution to  $\langle d_s g_n(s, \bar{s}) \rangle_{s \in \mathcal{S}}$ , and a negative contribution to  $M_0$ .

Combining the approximations of both contributions to the first line of Eq. (17), we obtain Eq. (??) of the main text. This expression provides a fair estimate of  $M_0$ , as shown in Fig. 5.

### E. Approximate expression of $M_*$

Assuming for the sake of simplicity complete uncorrelation between  $u_{ss'}$  and  $\tau_\infty(s', \bar{s})$ , the covariance  $|d_s g_u(s, \bar{s})|$  can be approximated as the product of the standard deviations  $\sigma_u$  and  $\sigma_{\tau_\infty}(\bar{s})$  of  $u_{ss'}$  and  $\tau_\infty(s, \bar{s})$  in  $\mathcal{B}_s$ , times the absolute value of a sum of  $d_s$  random signs that account for the possible signs of the products. This sum is approximated by the standard formula for the expectation value of the absolute distance after  $d_s$  steps as  $(2d_s/\pi)^{1/2}$  [5]. As a consequence, we have

$$|d_s g_u(s, \bar{s})|_{s \in \mathcal{S}} \approx (2/\pi)^{1/2} \langle d_s^{1/2} \rangle_{s \in \mathcal{S}} \sigma_u \sigma_{\tau_\infty}(\bar{s}). \quad (21)$$

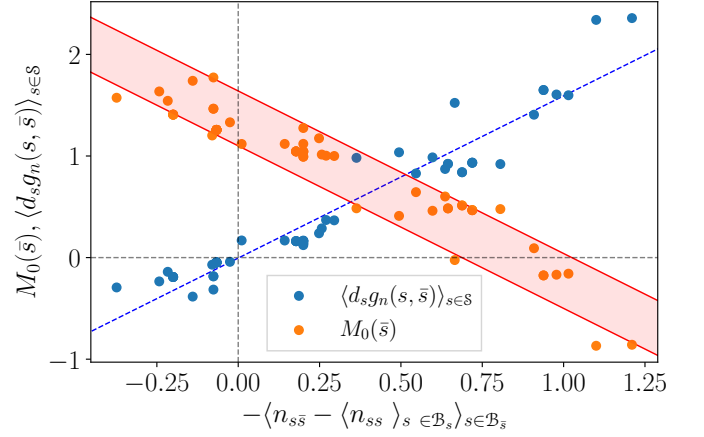


Figure 5.  $M_0(\bar{s})$  and mean of  $d_s g_n(s, \bar{s})$  over all states as a function of the quantity  $-\langle n_{s\bar{s}} - \langle n_{ss''} \rangle_{s'' \in \mathcal{B}_s} \rangle_{s \in \mathcal{B}_{\bar{s}}}$  (the mean is taken over the bordering states of the target  $\bar{s}$ ). The blue dashed line is a fit of  $\langle d_s g_n(s, \bar{s}) \rangle_{s \in \mathcal{S}}$ , that gives a slope  $\rho_1 \approx 1.60$ . This value is used to draw the two red lines, which correspond to the approximate relation  $M_0^{\text{appr}}(\bar{s}) = \rho_0(N) - \rho_1 \langle n_{s\bar{s}} - \langle n_{ss''} \rangle_{s'' \in \mathcal{B}_s} \rangle_{s \in \mathcal{B}_{\bar{s}}}$ , with  $\rho_0(N = 3) = 1.1$  and  $\rho_0(N = \infty) = 1.64$  (the minimum and the asymptotic value of  $\langle n_{ss'} \rangle_{s' \in \mathcal{B}_s}$ , see Fig. 3).

As shown in Fig. 6, this expression provides a fair approximation to  $\langle |d_s g_u(s, \bar{s})| \rangle_{s \in \mathcal{S}}$ . The averages  $\langle u_{ss'} \rangle_{s' \in \mathcal{B}_s}$  are small and their contribution to the term  $\langle |(1 - \delta_{s\bar{s}}) \langle u_{ss'} \rangle_{s' \in \mathcal{B}_s} - d_s g_u(s, \bar{s})| \rangle_{s \in \mathcal{S}}$  is negligible. This is also shown in Fig. 6, where the difference between  $\langle |d_s g_u(s, \bar{s})| \rangle_{s \in \mathcal{S}}$  and  $\langle |d_s g_u(s, \bar{s}) - \langle u_{ss'} \rangle_{s' \in \mathcal{B}_s}| \rangle_{s \in \mathcal{S}}$  is seen to be small.

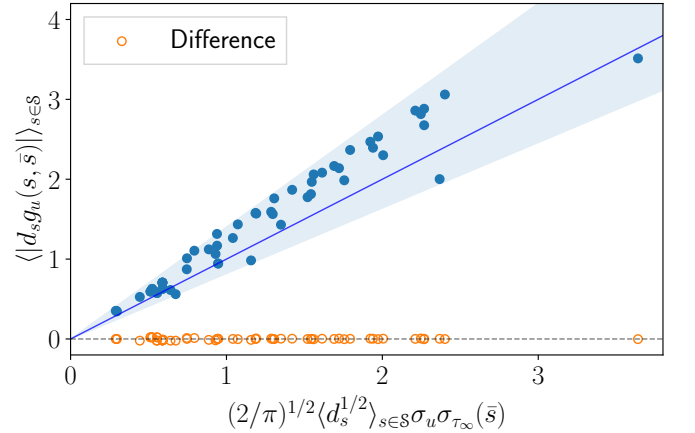


Figure 6. Blue dots: mean of the covariance  $|d_s g_u(s, \bar{s})|$  over all states as a function of its approximation Eq. (21). The orange dots are the difference between  $\langle |d_s g_u(s, \bar{s})| \rangle_{s \in \mathcal{S}}$  and  $\langle |d_s g_u(s, \bar{s}) - \langle u_{ss'} \rangle_{s' \in \mathcal{B}_s}| \rangle_{s \in \mathcal{S}}$ .

Finally, in Figs. 2 and 7, we show that the standard deviation  $\sigma_u$ , which is bounded, converges to a constant roughly equal to 0.44, while the quantities  $\sigma_{\tau_\infty}(\bar{s})$  and  $\langle d_s^{1/2} \rangle_{s \in \mathcal{S}}$  grow with  $N$ .

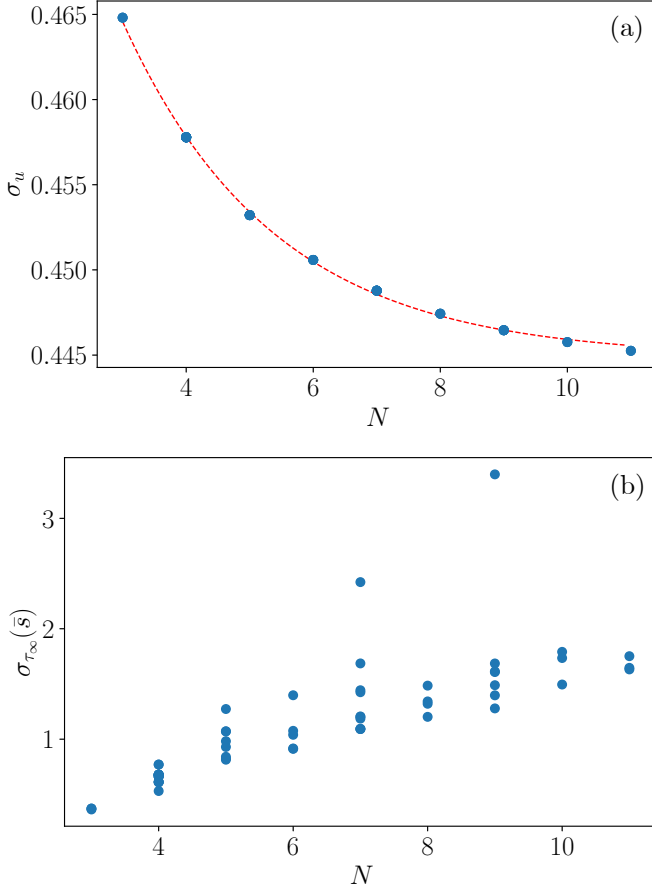


Figure 7. (a) Standard deviation  $\sigma_u$  as a function of  $N$ . The points are fitted with a decreasing exponential, which gives an asymptotic value approximately equal to 0.44. (b) Standard deviation  $\sigma_{\tau_\infty}(\bar{s})$  for different targets as a function of  $N$ .

### III. ZERO-FORCE VS RANDOM POLICY

To calculate the gain in the expected return time to target due to the optimization, we use the zero-force policy as a reference. However, using a random-force policy leads to similar results: in Fig. 8 the return time to target for the zero-force and the random policy for three different targets are seen to lead to similar values of  $\tau_\phi^r(\bar{s})$ .

### IV. OPTIMAL RETURN TIME TO TARGET FOR BIG TARGETS

For big targets, we expect  $M_*(\bar{s})$  to be negative and thus to observe a minimum in the optimal return time to target  $\tau^r(\bar{s})$ . This is confirmed by Fig. 9, where  $\tau^r(\bar{s})$  is plotted as a function of  $1/T$  for seven targets with  $N = 12$  and  $F_0 = 0.4$ .

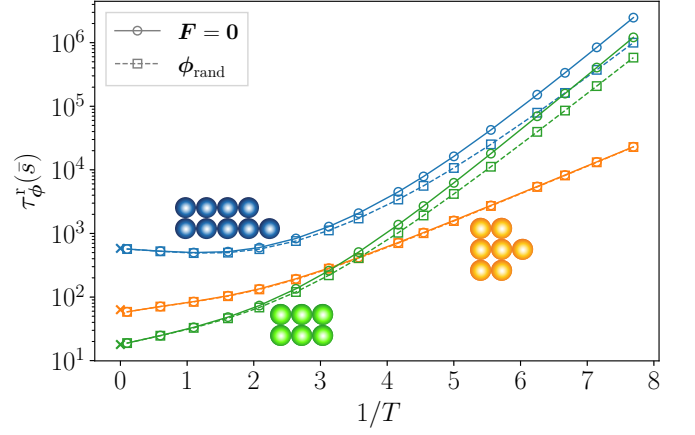


Figure 8. Expected return time to target  $\tau_\phi^r(\bar{s})$  for the zero-force case and under a random policy  $\phi_{\text{rand}}$  (i.e. a policy that chooses a random force with equal probability in each state) for the three targets shown in the figure, as a function of  $1/T$ .

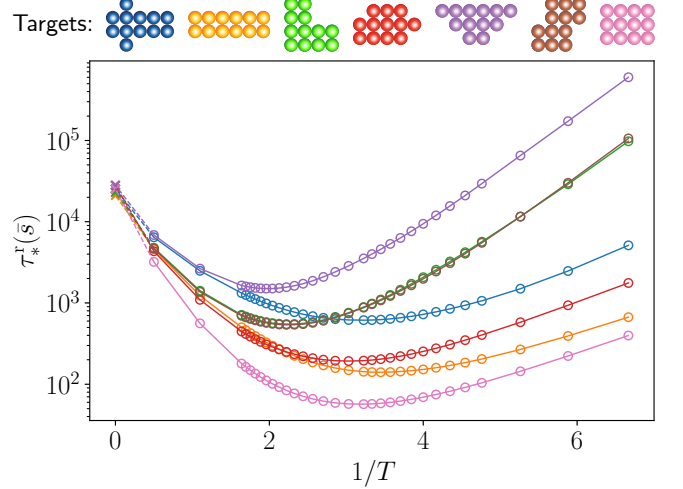


Figure 9. Optimal return time to target  $\tau^r(\bar{s})$  as a function of  $1/T$  for targets with  $N = 12$ . All the curves exhibit a minimum, corresponding to an optimal temperature. The  $\times$  correspond to the analytical expression of  $\tau_\infty^r(\bar{s})$  for  $T \rightarrow \infty$ .

### V. COMPUTATION TIME AS A FUNCTION OF CLUSTER SIZE

In Fig. 10, we report measurements of the computation time required to obtain an optimal policy with value iteration for several targets of size  $4 \leq N \leq 12$ , at two different temperatures  $T = 0.15$  and  $T = 0.59$ . The amplitude of the force is  $F_0 = 0.4$ . In both cases, the time increases exponentially as  $\sim 6^N$ . The computations have been performed with a sequential code on two different computers, with processors Intel Xeon E5-1650 3.50GHz and Intel Xeon E5-2630 2.40GHz.

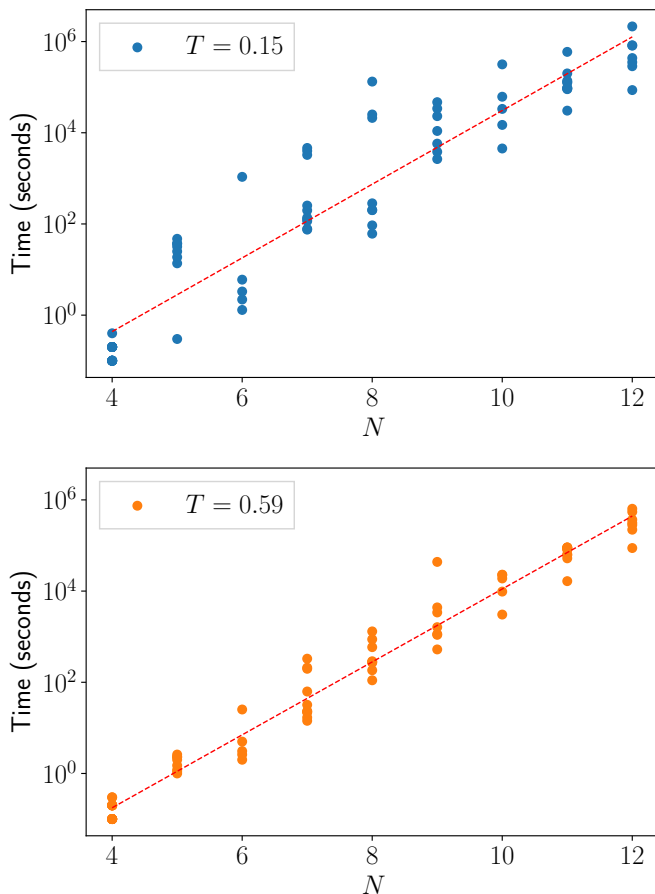


Figure 10. Computation time to obtain an optimal policy as a function of cluster size  $N$ , for several targets of size  $4 \leq N \leq 12$ , at  $T = 0.15$  and  $T = 0.59$ .

## VI. EFFECT OF FREEZING ATOMS WITH 4 NEAREST NEIGHBORS

In Fig. 11 we show a comparison of the mean return time to target  $\tau_*^r(\bar{s})$  calculated when freezing atoms with 4 nearest neighbors (as in the results of the main text), and when unfreezing them, for two targets with  $N = 7$  and  $N = 8$ . Note that, for  $N \leq 6$ , there is no difference between the two cases, since there are no configurations that allow a displacement of an atom with 4 nearest

neighbors, without leading to cluster breaking (which is forbidden in our model).

While the results are always accurate at low temperature, some deviations are found at high temperatures. The maximum deviation at high temperature is around 3% in Fig. 11(a), and around 45% for the 8-particle target with a hole in Fig. 11(b). Indeed, in this latter target the reverse moves of the 8 moves bringing a particle to the empty center of the cluster are forbidden by the freezing of particles with 4 nearest neighbors.

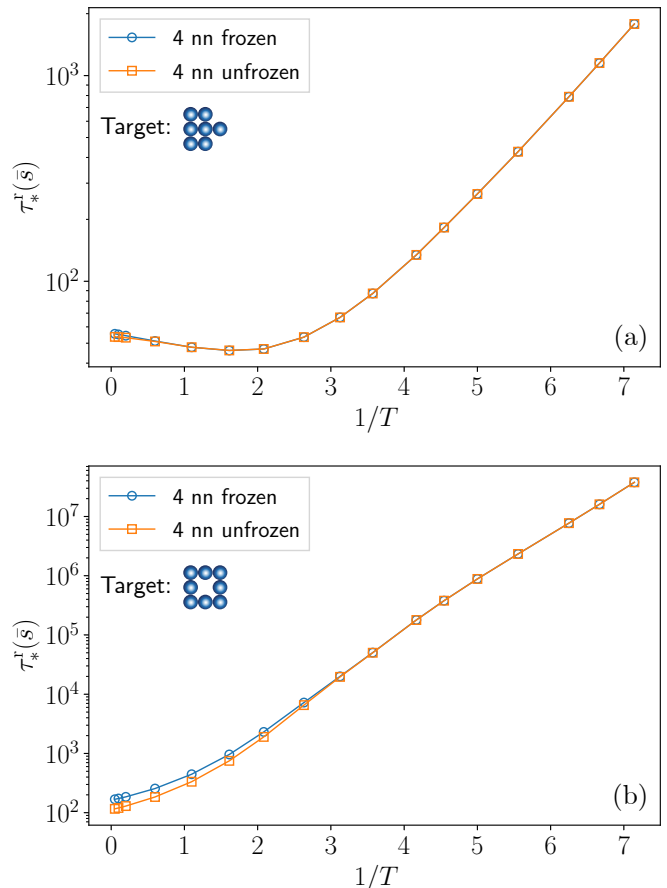


Figure 11. Comparison of the mean return time to target  $\tau_*^r(\bar{s})$  as a function of temperature for the case where the atoms with 4 nearest neighbors are frozen and the case where they are unfrozen, for (a) a 7-atom and (b) a 8-atom target.

- [1] J. D. Noh and H. Rieger, Phys. Rev. Lett. **92**, 118701 (2004).
- [2] A. Baronchelli and V. Loreto, Phys. Rev. E **73**, 026103 (2006).
- [3] Y. Lin, A. Julaiti, and Z. Zhang, J. Chem. Phys. **137**, 124104 (2012).
- [4] V. Tejedor, O. Bénichou, and R. Voituriez, Phys. Rev. E **80**, 065104 (2009).
- [5] R. E. K. Mosteller, F.; Rourke and G. B. Thomas, *Probability and Statistics*. (Addison-Wesley, 1961).